Journal of Applied Fluid Mechanics , Vol. 9, No. 5, pp. 2311-2319, 2016.
Available online at www.jafmonline.net, ISSN 1735-3572, EISSN 1735-3645.
DOI: 10.18869/acadpub.jafm.68.236.24723

Turbulent Viscosity Concept Downstream an Open-Channel Sudden Expansion

L. Han, E. Mignot† and N. Rivière

LMFA, CNRS-Université de Lyon, INSA de Lyon, Bat. Joseph Jacquard, 20 Av. A. Einstein, 69621 Villeurbanne, France.

† *Corresponding Author Email*: *emmanuel.mignot@insa-lyon.fr*

(Received February 19, 2015, ; accepted October 27, 2015,)

ABSTRACT

The recirculations are essential in river engineering because they form silting zones and favour the development of specific fauna and flora. This paper deals with the behaviour of the recirculation zones occurring downstream the sudden expansion of an open channel. An Acoustic Doppler Velocimeter is used to measure the flow details. The mean flow property such as the length of the recirculation, the average velocity field and velocity gradient are obtained. Then the self-similarity of the velocity profile is retrieved . The numerical simulation for the similar conditions are preformed with the CFD software STAR CCM+. When compared with the experiments, the two approaches correspond well in terms of length of recirculation zone and also regarding details such as the velocity gradient profiles. Finally, the eddy viscosity concept is tested and the turbulent viscosity coefficient are obtained along the streamwise axis for all flows.

Keywords: Shallow flow; Turbulent eddy viscosity; Experiments; Numerical simulation; Recirculation.

NOMENCLATURE

B	channel entire width
c_f	skin friction coefficient
d	expansion width
h	water depth
L	length of the recirculation zone
L_b	length of the upstream part
L_t	length of the whole channel
Q	discharge of the flow
R_b	expansion ratio
S	bed friction number
U	streamwise time-average velocity
V	transverse time-average velocity
y_c	mixing layer center
δ	width of the mixing layer
ε	equivalent roughness height
ε_0	dimensionless turbulent viscosity
λ	Darcy-Weisbach friction coefficient
μ_T	dynamic turbulent eddy viscosity
ν_T	kinematic turbulent eddy viscosity

1. INTRODUCTION

A shallow open channel corresponds to a configuration where the horizontal dimensions are much larger than the vertical extent so that the vertical component of the flow acceleration is negligible compared with the horizontal acceleration components (Liang 2006). These flows correspond to very common phenomena in the nature, such as wide rivers, coastal lagoons or estuaries (Babarutsi *et al.* 1989). Consequently, shallow recirculating flows also commonly occur and are observed in bays and harbors (Ouellet *et al.* 1986), behind islands (Wolanski and Heron 1989), natural streams in rivers and estuaries (Chu *et al.* 2004). Li and Djilali (1995) and Mignot *et al.* (2014)(b) have illustrated many common geometries of recirculation zone including sudden expansions, backward facing steps, or flows around obstacles such as cylinders. The recirculation downstream sudden expansions is one among all of them. It has significant implications in terms of sediment or passive scalar exchanges (Babarutsi and Chu 1991)

between the main flow and the dead zone where silting occurs (Rivière *et al.* 2011). This dead zone favors the development of specific fauna and flora thanks notably to the exchanges of oxygen, nutrients and other fundamental components through its boundary which is a mixing layer (Kimura and Hosoda 1997,Uijttewaal and Booij 2000).

For a free and straight mixing layer, (Wygnanski and Fiedler 1970) show that a maximum turbulent activity takes place along the centerline and that the width of the mixing layer linearly increases. However, for the more complex mixing layer occurring at the boundary of a recirculation, (Talstra 2011) shows that the width of the mixing layer first increases along the streamwise direction and then becomes a plateau near the end of the recirculation. Another complexity is introduced herein as some of our mixing layers are shallow. To characterize this shallowness, a parameter named bed friction number S was introduced by Chu *et al.* (1983) based on the stability analysis of the depth-averaged shallow water equation and by Chu *et al.* (1991) considering a turbulent kinetic energy balance. S is defined as the ratio between the dissipation term due to bottom friction and the production term due to transverse shear across the mixing layer. Using a classical inviscid theory , a critical bed friction number S_c=0.12 is found by Chu *et al.* (1983). It means that in shallow condition where S_c >0.12, the bottom friction impedes the growth of the instabilities and in deep condition (S_c <0.12), the bottom friction effect remains negligible. Based on measurements of the shallow mixing layer width growth rate, Chu and Babarutsi (1988) found S_c=0.09 while Uijttewaal and Booij (2000) propose S_c=0.08. Uijttewaal and Booij (2000) proved that the shallowness limits the growth of the large scale eddies in the vertical direction so that these eddies become quasi-2D. It can then be assumed that the eddy viscosity will also be influenced by the shallowness. Babarutsi *et al.* (1989) applied this concept to the shallow sudden expansion and formulated $S = \lambda d/8h_0$ where λ is the Darcy-Weisbach friction coefficient, d is expansion width and h_0 is the water depth, as seen in Fig. 1.

The equation governing the fluid motion in a turbulent flow is the classical Reynolds Averaged Navier-Stokes equation (RANS). A simple way of solving the RANS equation is to relate the Reynolds stress tensor to the mean flow characteristics namely the classical Boussinesq′s hypothesis, which is used in many different fields to model turbulent flows (Schimitt 2007). It is based on an equivalence between the Reynolds shear stress and mean strain tensors (*e.g.* the time-averaged velocity gradient). In such case, the coefficient of proportionality is termed the eddy viscosity μ_T, which is far from being a constant or fluid property. Mignot *et al.* (2014)(a) reveal that the eddy-viscosity concept fairly predicts the Reynolds shear stress (see their Fig. 12) in the recirculation of an open channel bifurcation. However, few works focus on the influence of the shallowness on the eddy viscosity.

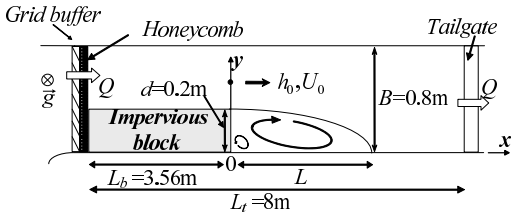

Fig. 1. Plan view of the experimental facility and the configuration of the expansion.

As a consequence, the aim of the present work is to investigate the turbulent viscosity in the mixing layer produced by the sudden expansion for very different flows with different shallowness, *i.e*, different bed friction number S. After presenting the experimental set-up and the numerical model, the results are discussed regarding the impact of shallowness on the flow characteristics, on the Reynolds stress tensor and on the eddy viscosity.

2. EXPERIMENTAL AND NUMERICAL APPROACHES

2.1 Experimental Facility

Experiments presented in this paper were conducted in a straight open-channel flume located in the Laboratory of Fluids Mechanics and Acoustics (LMFA) of Lyon, France. This flume (length L_t=8m and width B=0.8m) is straight, has a symmetrical rectangular cross-section and a streamwise mean slope of 0.18%.The channel is PVC made and its surface typical roughness is $\varepsilon = 5 \times 10^{-5}$m. Geometrical parameters are sketched in Fig. 1. A rectangular impervious block of PVC of width d=0.2m is constructed along the upstream part of the right bank over a length L_b=3.56 m. The expansion ratio thus equals R_b=(B-d)/B=0.75. The axis system is set as depicted on Fig. 1 with the origin ($x = 0$, $y = 0$) located at the expansion section along the right side wall, where x represents the streamwise axis and y is the crosswise axis. A grid buffer and a honeycomb are used for stabilizing the inflow upstream. Moreover, a float board made of ex-

Fig. 2. The structure of the side-looking ADV and the sampling volume working principle. From the user guide of Nortek, 2004.

truded polystyrene lies on the water free surface in order to release the oscillations on the flow. The downstream boundary condition consists of an adjustable tailgate, allowing to precisely adjust the downstream water depth. The experiments include 4 flow conditions with discharges in different orders of magnitudes (see Table 1). Hence, two electromagnetic flowmeters (Endress-Hauser) are used herein, one for the range Q =5−40 L/s with an uncertainty 0.2L/s, another one for Q <5 L/s with an uncertainty of 0.025L/s. The velocity field is measured using a Vectrino+ Nortek side-looking ADV (Acoustic Doppler Velocimeter)(see Fig. 2). In shallow conditions, this device permits to access the two horizontal velocity components u along the streamwise x and v along transverse y directions respectively. The side-looking ADV (see Fig. 2) is mounted on an automatic displacement and recording carriage connected to a PC computer through LabVIEW software. Hollow glass spheres (50μm) and hydrogen micro-bubbles are added to the flow upstream. The ADV measurement grid is composed of about 1000 points which covers the entire recirculation region (0< x <1.3L with L the recirculation length and 0< y <3.5d).The water depth is measured using an ultrasonic probe also located on the automatic displacement carriage.

2.2 Data Post-Processing and Correction

ADV is quite convenient to use for characterizing both velocities and fluctuation, notably once mounted on the automatic traverse equipment. However, it presents two main disadvantages.

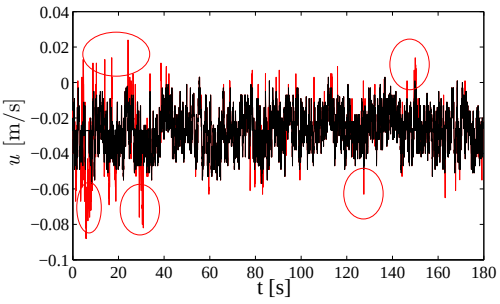

Fig. 3. A processed velocity signal (black −) without the peaks (the points in red ◯) seen on the original data (red −).

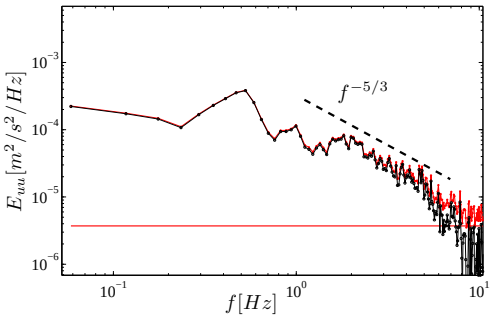

Fig. 4. A spectrum of the streamwise velocity u with the high frequency noise deleted (black .−) with comparison with the original spectra (red .−). −− is the Kolmogorov′s 5/3 Law.

The first one is aliasing of the signal emitted by the ADV. The phase-shift between the outgoing and incoming pulse introduces a spike in the recording data Goring and Nikora (2002), as shown in Fig. 3. The spikes are removed using a correction of the method developed by Goring and Nikora (2002). This method is called "Phase-Space Thresholding Method" and is widely used by most of the ADV users. It is clear that in Fig. 3 the processed signal is free of peaks.

The second disadvantage of the ADV is that Doppler noise appears at high frequencies and creates an additional variance that increases the turbulent intensity (Nikora and Goring (1998) and Voulgaris and Trowbridge (1997)). Here the spectrum analysis is used for detecting and deleting the noise. In Fig. 4, some high frequency (f >7Hz) noises exist. When the noise is deleted, the signal fits well with the Kolmogorov′s -5/3 law.

2.3 Numerical Approach

The RANS equations are solved using a 3D numerical model (StarCCM+) using a $k-\varepsilon$

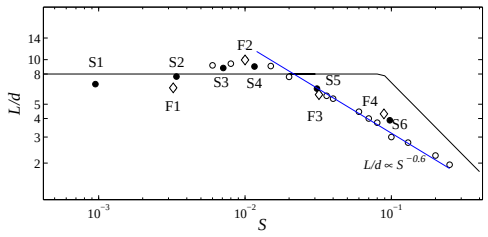

Fig. 5. Evolution of the non-dimensional recirculation length L/d as a function of the friction number S with: 4 selected configurations deeply studied in the sequel (marker ◇: See Table 1); ○: the additional experimental configurations and ●: the numerical results. The black lines − are the asymptots proposed by Babarutsi *et al.* (1989).

turbulent closure scheme. This approach considers the following simplifications:

1. A constant water depth using a rigid-lid method (Plane wall with slip condition) in the calculation while the water depth evolves in the experiment. It was verified that the recirculation length obtained with this simplification compares well with both the experiments (see Fig. 5) and simulations using the VOF method, but with a much smaller computational cost.

2. An isotropic turbulence model is used for the turbulent closure. The realizable $k-\varepsilon$ model is chosen. This can be surprising as other models such as $k-\omega\,SST$ proved to be more accurate for the classical backward-facing step case. Nevertheless, during preliminary tests, realizable $k-\varepsilon$ model proved to be globally more accurate on the entire range of bed friction number S considered in this study. This was attributed to the influence of the vertical confinement between the bed and the free-surface, accounted by S. Moreover, an isotropic eddy viscosity, as considered in this model, is consistent with the approach adopted in the sequel of this paper (section 5.2).

3. FLOW PROPERTIES WITH VALIDATION OF SIMULATION

3.1 Length of the Recirculation

The length of the recirculation zone L/d is the characteristic we consider of primary importance in this study. For the condition R_b=0.75, the dimensionless lengths of the recirculation L/d are given in Fig. 5.

Table 1 Flow characteristics for all studied configurations of experiments and calculations with U_0 and h_0 the bulk velocity and the water depth at the expansion x=0

Test	U_0(m/s)	h_0(m)	S	L/d
F1	0.23	0.156	0.0032	6.45
F2	0.55	0.050	0.01	9.95
F3	0.36	0.021	0.032	5.80
F4	0.20	0.022	0.089	4.3
S1	0.32	0.4	0.001	6.84
S2	0.74	0.1	0.003	7.69
S3	1.3	0.05	0.007	8.78
S4	2.1	0.03	0.012	8.98
S5	0.3	0.02	0.03	6.38
S6	0.6	0.01	0.098	3.89

Fig. 5 compares the experimental and numerical results. The qualitative trend is retrieved by the numerical approach:

− For large bed friction numbers S, L/d decreases as S increases.

− For $S\sim$0.01, L/d reaches a maximum value

− For small S values, L/d decreases as S decreases.

To conclude, the numerical code appears to fairly estimate the recirculating length and is in agreement with the evolution of L/d for varying S values. This numerical approach can then be used for further analysis.
When comparing with the asymptotes proposed by Babarutsi *et al.* (1989), it is clear that the experimental and numerical data shows the same decreasing tendency for high S value (Shallow flows). Oppositely, but in the region of small S values (in deep condition), L/d decreases as S decreases which is a quite different result.

3.2 Mean Velocity Property

For further studying the mixing layer characteristics, 4 experimental configurations F1-F4 (see Table 1) and one numerical configuration S5 were tested.

The mean velocity fields are shown in Fig. 6 (experiments) and Fig. 7 (numerical simulations). The four experimental configurations give the same tendency:

1. The flow separates near x/L=0 and y/d=1, with a velocity vector almost parallel to the x axis.

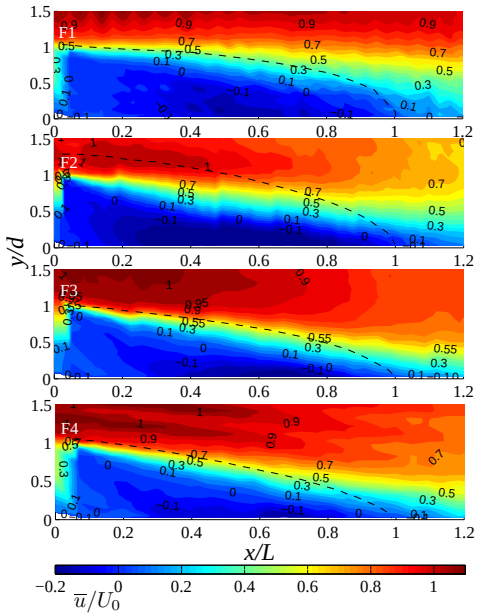

Fig. 6. Contours of the mean streamwise velocity $\overline{u}/U_0$ with the streamline −− which ends at the reattachment (Experiment).

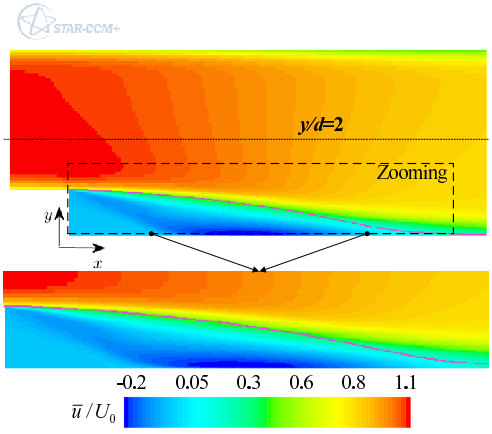

Fig. 7. Contours of the mean streamwise velocity $\overline{u}/U_0$ for S5 with the streamline − which ends at the reattachment (Simulation).

2. The flow reattaches at x/L=1 where the mean streamwise velocity close to the wall changes sign from negative to positive.

3. A main recirculation structure forms for y/d <1 and x/L <1 and a secondary cell near the corner at x=y=0 can also be observed (especially for F2).

4. The streamlines which end at the reattachment point $x/L = 1$ exhibit the same pattern and interact with the side wall at the position where $\overline{u} = 0$

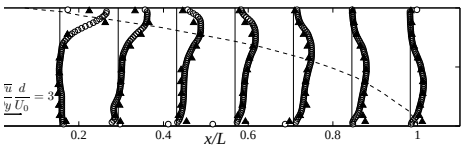

Fig. 8. Evolution of the transverse gradient of mean streamwise velocity. ▲ is the experimental data (F3) and ∘ is the simulation data (S5, more dense than experiment). Line −− is the streamline of F3.

The simulation configuration S5 corresponds well with the experiment F3 as shown in Fig. 6 and Fig. 7. The recirculation zone is well developed in the region 0< x/L <1. The velocity in outer region (y/d >2) decreases along the streamwise direction as a consequence of the expansion.

Velocity gradient profiles for configurations F3 and S5 are plotted in selected sections x/L in Fig. 8. Again a fair agreement is obtained between the experiments and simulations globally except for some points in the lateral wall from 0.4< x/L <0.6. It appears that the maximum gradient takes place along the separating streamline (experiment) for x/L <0.8, and that further downstream the maximum gradient remains far from the side wall while the separating streamline reattaches. Moreover, it appears that the magnitude of maximum gradient of each section decreases towards the reattachment point.

3.3 Similarity

Many studies in the literature showed that the transverse profiles of mean streamwise velocity are self-similar (see for instance, Bell and Mehta (1990) for a free unbounded mixing layer, Mignot *et al.* (2014)(b) for a confluence, or Lyn and Rodi (1994) for the flow over an obstacle). This behaviour is also retrieved in our flows with $(\overline{u}-U_2)/(U_1-U_2)$ plotted as a function of $(y-y_c)/\delta$ in Fig. 9 with:

1. $U_1(x)$ is the outer velocity magnitude in the free stream, measured at y/d=1.5 for each section.

2. $U_2(x)$ is the outer velocity on the recirculation side, which is defined as U_2=0 as proposed by Talstra (2011).

3. y_c is the maximum transverse gradient position at each section x/L.

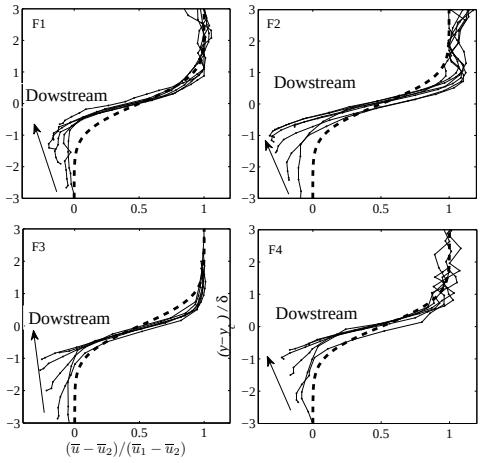

Fig. 9. Mean streamwise velocity profiles in similarity coordinates for the four cases F1 to F4. The locations of the velocity profiles are regularly spaced as in Fig. 8. −−is the Gaussian curve.

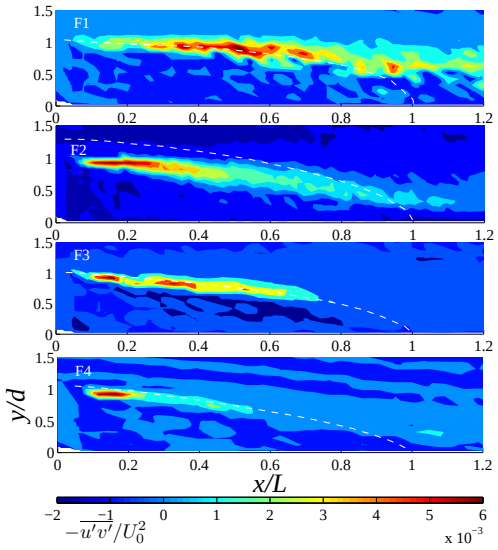

Fig. 10. Evolution of the Reynolds shear stress term: $-\overline{u'v'}$ normalised with U_0^2. Note: the white −− line is the separating streamline.

4. δ is the width of the mixing layer which equals $\delta(x) = \frac{U_1(x)-U_2(x)}{|\frac{\partial \overline{u}(x)}{\partial y}|_{max}}$

The agreement is fair over about two mixing layer widths ($y - y_c = \pm\delta$). The dash lines in the figures are the Gaussian curve plus a constant, as proposed by Lyn and Rodi (1994). The agreement is good in the outer side of the mixing layer and satisfactory in the region of the recirculation. Along the streamwise direction x, the measurements separate from the Gaussian curve for the four configurations where $(y-y_c)/\delta$ <-1.

4. TURBULENT CHARACTERISTICS

Figure 10 plots the Reynolds shear stress $-\overline{u'v'}$ in color contour.

It appears that the shear stress distributions are quite qualitatively similar for the 4 measured flows:

1. In the upstream region, the maximum Reynolds shear stress is located along the streamline and decreases towards the side wall ($y/d = 0$) and the outer region (y/d >1).

2. In the downstream region (x/L >0.8), the maximum Reynolds shear stress is located away from the side wall.

3. The shear stress magnitudes increase in the upstream region of the mixing layer and reach a maximum value at $x/L \sim 0.2$ to 0.5 and then decrease downstream. Besides, the position of this maximum value moves upstream as S increases.

4. The region of elevated Reynolds shear stress becomes smaller as the bed friction number S increases.

As a consequence, the vertical confinement between the bed and the free surface affects the shear stress of the flow which impedes its development along the streamwise direction.

5. TURBULENT VISCOSITY CONCEPT

5.1 Gradient Model

The eddy viscosity concept, following the works of Joseph Boussinesq in 1877, relates the Reynolds stress tensor to the mean rate of strain tensor, it reads:

$$-\overline{u_i'u_j'} + \frac{2}{3}k\delta_{ij} = \nu_T(\partial\overline{u_i}/\partial x_j + \partial\overline{u_j}/\partial x_i) = 2\nu_T S_{ij} \quad (1)$$

with ν_T the so-called "turbulent viscosity" or "eddy viscosity" coefficient, k the turbulent kinetic energy, δ_{ij} the Kronecker symbol which equals to 1 if $i = j$ and 0 if $i \neq j$ and finally S_{ij} the mean rate of strain tensor.
Here, ν_T is hypothesized isotropic as it does not depend on i and j, and it is not satisfied in many configurations (see (Pope 2008)). So it is not expected to be valid in the present flow configuration, and no discussion regarding the validity of the isotropic turbulent viscosity assumption

is made here. This paper is based on a two-dimensional (2D) analysis, application of Eq.1 to the non-diagonal term becomes:

$$-\overline{u'v'} = \nu_T(\frac{\partial \overline{u}}{\partial y} + \frac{\partial \overline{v}}{\partial x}) = 2\nu_T S_{xy} \quad (2)$$

Note that in our flows, $\frac{\partial \overline{u}}{\partial y} >> \frac{\partial \overline{v}}{\partial x}$ (not shown here), Eq.2 thus simplifies as below:

$$-\overline{u'v'} = \nu_T(\frac{\partial \overline{u}}{\partial y}) \quad (3)$$

5.2 Estimation of ν_T Coefficient

Figure 10 and Fig. 8 reveal that the Reynolds shear stress and velocity gradient terms exhibit a similar qualitative pattern. This gives credit to the application of the eddy viscosity concept. In order to test the validity of the simplified gradient model (Eq. 3), the dimensionless $-\overline{u'v'}$ and $\nu_T(\frac{\partial \overline{u}}{\partial y})$ are plotted together on Fig.11 with ν_T calculated as the best-fit for each transverse section with the least square method (noted $\nu_{T-best\,fit}$). It reveals that for the 4 flows, the agreement is fair. Note that, due to some perturbation (which origin remains unknown) of the Reynolds shear stress term near the reattachment section, agreement there is not obtained. Nevertheless, the overall agreement is fair. $\nu_T(x)$ obtained by the best-fit are shown in Fig. 12: for the 4 flows, the terms $-\overline{u'v'}$ and $\nu_T(\frac{\partial \overline{u}}{\partial y})$ show the same tendency with a maximum located at the same y/d position and a decrease along both sides. It confirms that $\nu_T(x)$ does not varies much along the streamwise direction. For instance for flow F2 it varies between 2×10^{-4} and $1.5\times10^{-4}\,m^2/s$, that is $\pm14\%$ around the mean value.

The average value of $\nu_T(x)$ of all the sections is refered to as $\nu_{T-Global}$ in Table 3. In Fig. 13, the application of $\nu_{T-best\,fit}$ and $\nu_{T-Global}$ are compared at two x/L sections. In the upstream region of the recirculation zone (x/L=0.1), the two terms are in fair agreement. In the downstream region of the recirculation zone (x/L=0.9), the two definitions are in acceptable agreement. Hence, for the further analysis, only $\nu_{T-Global}$ will be considered for its simpler use.

Obtained values of $\nu_{T-Global}$ are listed in Table 2 along with values obtained from the numerical simulations ν_{T-Simu} (averaged also on all the sections). These values are of the same order of magnitude. Especially, configurations F1, F3 and F4 exhibit similar quantitative values between experiment and simulation. For F2, the values differ between experiments and simulation because the two points are not exactly in the same condition.

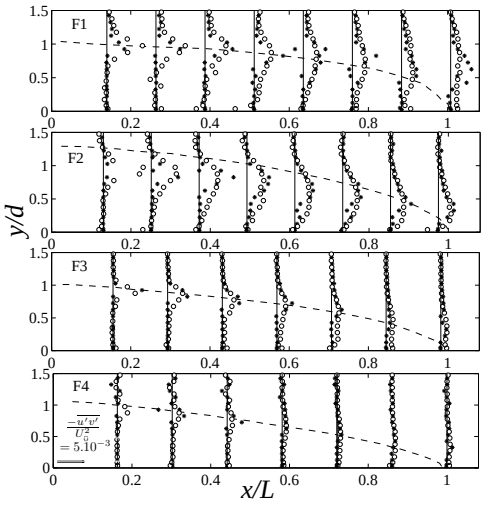

Fig. 11. Evolution of Eq.3 in each profiles normalized with U_0^2. Note the ∘ is the $\nu_T(\frac{\partial \overline{u}}{\partial y})$ and the ∗ is the $-\overline{u'v'}$.

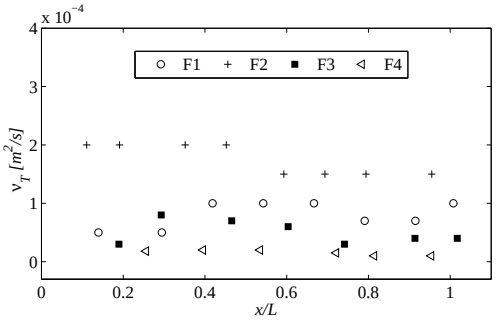

Fig. 12. The best fit turbulent viscosity magnitude $\nu_{T-Best\,fit}(x)$ along the streamwise for the 4 experimental cases.

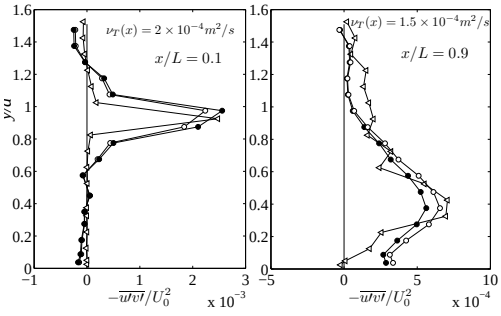

Fig. 13. Profiles of $\nu_T(\frac{\partial \overline{u}}{\partial y})$ using $\nu_{T-best\,fit}$ (∘) and $\nu_{T-Global}$=1.8×10^{-4} (•), compared with the shear stress term $-\overline{u'v'}$ (◁) for F2 at two streamwise section.

Table 2 $\nu_{T-Global}$ magnitude for the four experimental cases and the four corresponding numerical configurations

Cas Exp.	S	$\nu_{T-Global}$ $(10^{-4}m^2/s)$	Case Num.	ν_{T-Simu} $(10^{-4}m^2/s)$
F1	0.0032	0.8	S2	0.6
F2	0.01	1.75	S4	4.7
F3	0.032	0.5	S5	0.4
F4	0.089	0.155	S6	0.2

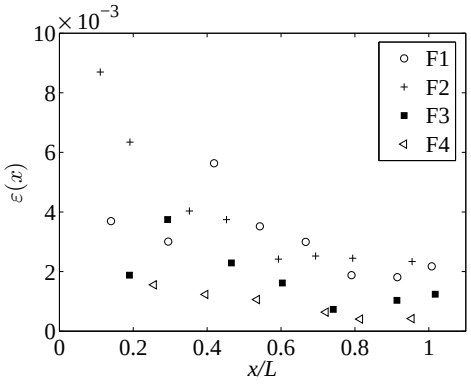

Fig. 14. The dimensionless turbulent eddy viscosity coefficient $\varepsilon(x)$ in the region of recirculation.

5.3 The Dimensionless Turbulent Viscosity

For further studying the bed friction influence on the turbulent viscosity, the dimensionless turbulent eddy viscosity coefficient $\boldsymbol{\varepsilon_0}$ is introduced here. (Tennekes and Lumley 1972) and (Wygnanski and Fiedler 1970) defined it as $\varepsilon_0 = \nu_T/\Delta U\delta$. In the recirculation flow, the selected characteristic scales for normalising are $\boldsymbol{\delta(x)}$ and $\boldsymbol{\Delta U = U_0}$. $\boldsymbol{\varepsilon(x)}$ is then defined as:

$$\varepsilon(x) = \frac{\nu_{T-Best\,fit}(x)}{\delta(x)U_0} \tag{4}$$

and $\boldsymbol{\varepsilon_0}$ is the spatially average value of $\boldsymbol{\varepsilon(x)}$ in the region $0 < \boldsymbol{x/L} < 1$.

Figure 14 reveals that $\varepsilon(x)$ decreases along the streamwise direction. Secondly, the value are in the same order of magnitude. Hence, for obtaining the region average value of the turbulent eddy viscosity, the arithmetic mean is used for the four experimental flows and the 6 numerical simulation from Table 1. The results are given in Fig. 15. It reveals that in the shallow region ($S > 0.01$), the experiments and the simulation fairly agree with each other. And more, the tendency is about $\propto S^{-0.6}$, which corresponds to the results obtained for L/d in Fig. 5. The difference between the experiments and the simulation increases for $S < 0.01$.

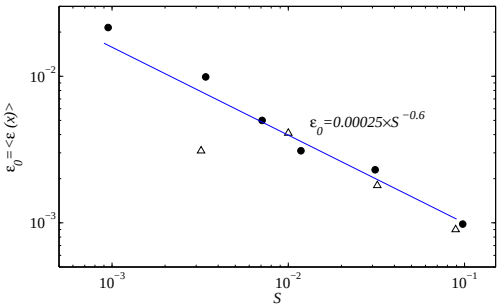

Fig. 15. The spatially average dimensionless turbulent eddy viscosity coefficient $\boldsymbol{\varepsilon_0}$ in the recirculation. Note that: △ are the experiment points(F1-F4) and the • are the simulation results (S1-S6).

6. Discussion and Conclusion

This paper focuses on the turbulent eddy viscosity characteristics occurring at the interface between the main flow and the recirculation zone created by a sudden expansion. The four different configurations differ in terms of shallowness S. Precise and exhaustive velocity field measurements were performed using an ADV for four experimental cases. In the same time, calculations are performed through numerical simulations using STAR CCM+. The main conclusions are:

(1) For the global characteristic of the expansion flow, *i.e.* the dimensionless length of the recirculation zone L/d, and for the details of the flow such as velocity gradients, the numerical results are in fair agreement with the experimental results.

(2) The turbulent characteristics in the mixing layer show strong similarities between the Reynolds shear stress and the velocity gradient profiles. This reveals the interest of testing the eddy viscosity concept.

(3) The gradient model is adapted to our experiments. It fairly applies for the four experimental cases. Secondly, the eddy viscosity remain nearly constant along the streamline.

The paper introduces the discussion regarding the dimensionless turbulent eddy viscosity coefficient ε with simulation and experiment. The two method give similar conclusion and approve that the numerical turbulent model (isotropic, statistically stationary) is adapted in this fluid pattern. Besides, the shallowness appears to play an important role in this parameter value. The results indicate that as the bed friction number S increases, ε_0 decreases along S.

REFERENCES

Babarutsi, S. and V. Chu (1991). Dye-concentration distribution in shallow re-circulating flows. *J. Hydr. Engin.*. 117(5), 643–659.

Babarutsi, S., J. Ganoulis and V. Chu (1989). Experimental investigation of shallow recirculating flows. *J. Hydraul. Eng.*. 115(7), 906–924.

Bell, J. and R. Mehta (1990). Development of a two-stream mixing layer from tripped and untripped boundary layers. *AIAA J.*. 28(12), 2034–2042.

Chu, V. and S. Babarutsi (1988). Confinement and bed friction effects in shallow turbulent mixing layers. *J. Hydraul. Eng.*. 114, 1257–1274.

Chu, V., F. Liu and W. Altai (2004). Friction and confinement effects on a shallow re-circulating flow. *Journal of Environmental and Engineering Science*. 3(5),463–475.

Chu, V., J. Wu and R. Khayat (1983). Stability of turbulent shear flows in shallow channels. In *Proc. of the 20th Congress of IAHR*, Moscow, Russia, pp. 128–133.

Chu, V., J. Wu and R. Khayat (1991). Stability of turbulent shear flows in shallow channels. *J. Hydraul. Eng.*. 117(10), 1370–1388.

Goring, G. and V. Nikora (2002). Despiking acoustic doppler velocimeter data. *J. Hydraul. Eng.*. 128(1), 117-126.

Kimura, I. and T. Hosoda (1997). Fundamental properties of flows in open channels with dead zone. *Journal of Hydraulic Engineering 123*(2), 98–107.

Li, X. and N. Djilali (1995). On the scaling of separation bubbles. *JSME Int. J. Series B*. 38(4), 541–548.

Liang, Q. (2006). Shallow flow hydrodynamics. *www.staff.ncl.ac.uk/qiuhua.liang/Research*. The website of Newcastle University.

Lyn, D. and W. Rodi (1994). The flapping shear layer formed by flow separation from the forward corner of a square cylinder. *J. Fluid Mech.*. 267, 353–376.

Mignot, E., D. Doppler, N. Rivière, I. Vinkovic, J. Gence and S. Simoens (2014). Analysis of flow separation using a local frame axis: Application to the open-channel bifurcation. *J. Hydraul. Eng.*. 140(3), 280–290,(a).

Mignot, E., I. Vinkovic, D. Doppler and N. Rivière (2014). Mixing layer in open-channel junction flows. *Envir. Fluid Mech.*. 14(5), 1027–1041,(b).

Nikora, V. and D. Goring (1998). Adv measurements of turbulence: Can we improve their interpretation? *Journal of Hydraulic Engineering*. 124(6), 630–634.

Ouellet, Y., D. P. and A. Soulamani (1986). Modlisation d'un coulement tourbillonnaire en rgime permanent. *Canadian Journal of Civil Engineering*. 13(3), 310–318.

Pope, S. (2008). *Turbulence flows*. Cambridge, United Kingdom: Cambridge University Press.

Rivière, N., S. Gautier and E. Mignot (2011). Experimental characterization of flow reattachment downstream open channel expansions. In *Proceedings of the 34th World Congress of the International Association for Hydro- Environment Research and Engineering*, Brisbane, Australia, pp. 3745–3752.

Schimitt, F. (2007). About boussinesq's turbulent viscosity hypothesis: historical remarks and a direct evaluation of its validity. *Comptes Rendus Mcanique*. 335(9-10), 617–627.

Talstra, H. (2011). *Large-scale turbulence structures in shallow separating flows*. Ph. D. thesis, Technische Universiteit Delft, Delft, Netherlands.

Tennekes, H. and J. Lumley (1972). *A First Course in Turbulence*. Massachusetts: Cambridge University Press.

Uijttewaal, W. and R. Booij (2000). Effects of shallowness on the development of free-surface mixing layers. *Phys. Fluids*. 12(2), 392–402.

Voulgaris, G. and J. Trowbridge (1997). Evaluation of the acoustic doppler velocimeter (adv) for turbulence measurements. *J. Atmos. Oceanic Technol.*. 15, 272–289.

Wolanski, E.and Imberger, J. and M. Heron (1989). Journal of geophysical research: Oceans. *J. Geophys. Res.*. 89(C6), 10553-10569.

Wygnanski, I. and H. Fiedler (1970). The two-dimensional mixing region. *J. Fluid Mech.*. 41(2), 327–361.